The 9th European Congress on Computational Methods in Applied Sciences and Engineering
ECCOMAS Congress 2024
3–7 June 2024, Lisboa, Portugal

POSTBUCKLING ANALYSIS OF VARIABLE STIFFNESS LAMINATES VIA R-FUNCTION METHOD

PAOLA P. FOLIGNO, CHENG A. YAN AND RICCARDO VESCOVINI

Politecnico di Milano
Dipartimento di Scienze e Tecnologie Aerospaziali
Via la Masa, 34, 20156, Milan, Italy
e-mail: {paolapia.foligno,chengangelo.yan,riccardo.vescovini}@polimi.it

Key words: R-Functions, Ritz method, Variable stiffness laminates, Asymptotic-numerical method, Postbuckling analysis

Summary. An innovative approach, which is based on the combined use of the R-functions theory and the Ritz method, is proposed as an effective mean for studying the postbuckling response of variable stiffness plates. This formulation allows any complex geometry to be handled in a meshfree framework. In this context, the potential of the elastic tailoring of VS laminates can be exploited to obtain a better shaping of the stiffness distribution in a arbitrarily shaped domain, where load concentrations are of concern. The attracting features of the proposed approach rely on the reduced modeling time and the faster solution procedure due to the asymptotic approach. These benefits are illustrated with two exemplary test cases, where comparison in shown against Abaqus simulations.

1 INTRODUCTION

Over the past years, innovative variable stiffness (VS) laminates, in which the fibers can vary their orientation as a function of the planar position, have received increasing attention due to their improved thermo-mechanical response [1]. These VS laminates are associated with an increased number of degrees of freedom with respect to their straight-fiber counterpart. Fast formulations based on the Ritz method are nowadays available [1–8]. However, one typical restriction regards the shape of the domain.

More advanced formulations are thus needed to explore the potential of the elastic tailoring of VS laminates in the postbuckling field. In fact, complex domains are typically characterized by undesired load concentrations, e.g. in correspondence of cut-outs, that can lead to structural damages. In this context, the potential of VS laminates can be exploited to achieve a better shaping of the stiffness distribution and to redirect the load path in the presence of these load concentrations.

In addition, efficient analysis methods are of paramount importance to avoid a high computational burden: the asymptotic-numerical method (ANM) is a powerful strategy to overcome this issue. Nonlinear problems are usually solved via predictor-corrector algorithms, such as the Newton-Raphson routine. The solution process is incremental, meaning that the load is divided in load steps and then an iterative procedure is carried out within each incremental step. Therefore, at each iteration a linearized equation is solved. Such algorithms are very powerful and well established, yet the computational time is still large with respect to linear problems.

The ANM was proposed several years ago by Potier-Ferry and co-workers. In Ref. [11], the asymptotic-numerical method was developed to compute perturbed bifurcations. In subsequent works ([12–15]) the method was applied for the postbuckling solution of elastic plates and shells. A more recent work [16] illustrates a complete bibliography of the ANM algorithm, including application fields and many variants.
To meet the above mentioned issues, a semi-analytical formulation is presented, based on the Ritz method, the asymptotic-numerical method and the R-functions theory [9]. R-functions are here used to represent the panel geometry and to enforce the essential boundary conditions. Complex domains can be modeled provided they are obtained from the composition of primitive geometries. In addition, the R-functions are exploited to build the boundary functions for the Ritz approximation. Any set of boundary and thermo-mechanical loading conditions can be considered. Starting from the approach developed in [10], this work exploits the R-functions theory to investigate the potential given by the elastic tailoring of VS laminates in the postbuckling regime. Furthermore, the ANM is here combined with the Ritz strategy to further improve the computational efficiency, obtaining both an efficient modelling approach and an effective solution strategy.

2 FORMULATION

A formulation for the analysis of VS plates with complex geometries is presented hereafter. Firstly, a brief introduction to the R-functions is given. They are used to represent the panel geometry and enforce the boundary conditions. Furthermore, the plate model and the variable stiffness distribution are presented. Also, the application of the R-functions in the context of the Ritz method is discussed. Then, the asymptotic-numerical method is introduced.

2.1 R-functions theory

R-functions are functions whose sign is completely determined by the sign of their arguments. From a real-valued function $f = f(x_i)$, its Boolean companion function F can be defined as:

$$F\left(S_2(x_i)\right) = S_2\left(f(x_i)\right) \qquad S_2(x_i) = \begin{cases} 0 & x_i < 0 \\ 1 & x_i > 0 \end{cases} \tag{1}$$

being S_2 the binary operator. One has to be able to construct at least one R-function per branch, which is a group of R-functions sharing the same companion function. In this work, the following set of functions is selected to have a sufficiently complete set:

$$\begin{aligned} \bar{x} &= -x && \text{(negation } \neg \text{ x)} \\ x \wedge_0 y &= x + y - \sqrt{x^2 + y^2} && \text{(conjunction } x \wedge y\text{)} \\ x \vee_0 y &= x + y + \sqrt{x^2 + y^2} && \text{(disjunction } x \vee y\text{)} \end{aligned} \tag{2}$$

Complex domains can be constructed through the composition of primitive domains using the operators defined in Eq. 2. By defining the i-th primitive domain as:

$$\Sigma_i = S_2\left(\sigma_i(x_j)\right) \tag{3}$$

one obtains the function representing the domain as:

$$\begin{aligned} \Omega &= F\left(S_2\left(\sigma_i(x_j)\right)\right) && \text{Boolean} \\ \omega &= f\left(\sigma_i(x_j)\right) && \text{Real-valued} \end{aligned}$$

Hereafter, an example of the construction of a complex domain using the R-functions theory is discussed. The domain is a rectangular plate with dimensions a and b and a circular hole of radius R centered in (x_0, y_0). Three primitive domains are defined, see Figs. 1(a) - 1(c), whose functions read:

$$\sigma_1 = \frac{a^2 - x^2}{2a} \qquad \sigma_2 = \frac{b^2 - y^2}{2b} \qquad \sigma_3 = \frac{1}{2R}\left[R^2 - (x - x_0)^2 - (y - y_0)^2\right] \tag{4}$$

The final domain, shown in Fig. 1(d), is obtained by combining the three primitive domains through conjunction and negation operators:

$$\omega = (\sigma_1 \wedge_0 \sigma_2) \wedge_0 \overline{\sigma_3} \tag{5}$$

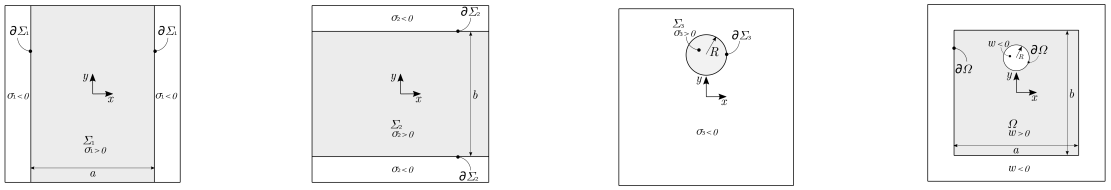

(a) (b) (c) (d)

Figure 1: Complex domain construction: a) vertical strip; b) horizontal strip; c) circular hole; d) final domain

2.2 Plate model

Variable stiffness laminates are considered in the present work. They are characterized by variable in-plane properties, with the fiber orientation varying across the domain. The fiber orientation is defined using Lagrange interpolation. A grid of points is considered, where the orientation angles are specified at arbitrary positions of the domain. The orientation angle in a generic point is evaluated as [17]:

$$\theta(x, y) = \sum_{m=0}^{M-1} \sum_{n=0}^{N-1} \theta_{mn} \prod_{m \neq i} \left(\frac{|x| - x_i}{x_m - x_i}\right) \times \prod_{n \neq j} \left(\frac{|y| - y_j}{y_n - y_j}\right) \tag{6}$$

Linear variation along x and y is retrieved as a special case by using two points only. The plate kinematics is modelled according to the First-order Shear Deformation Theory (FSDT). The relevant equations are not reported here for the sake of brevity, but can be found in Ref. [18]. The nonlinear strain components are approximated here according to von Kármán theory.

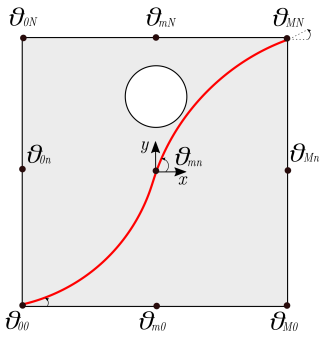

Figure 2: Fiber path

2.3 Numerical solution via Ritz Method

The numerical approximation refers to the Ritz method, which requires trial functions to be part of a complete set and satisfy essential boundary conditions. In order to satisfy completeness, Legendre polynomials are used. On the contrary, R-functions, that are null along the domain boundaries, are exploited to construct boundary functions in order to enforce kinematic boundary conditions. The generalized displacements are expressed as:

$$\begin{aligned} u_k(x,y) &= \omega_{u_k}(x,y)\left[\phi(x)^{\mathrm{T}} \otimes \psi(y)^{\mathrm{T}}\right]\mathbf{c}_{u_k} \qquad k = x,y,z \\ \varphi_\alpha(x,y) &= \omega_{\varphi_\alpha}(x,y)\left[\phi(x)^{\mathrm{T}} \otimes \psi(y)^{\mathrm{T}}\right]\mathbf{c}_{\varphi_\alpha} \qquad \alpha = x,y \end{aligned} \tag{7}$$

where $\mathbf{c}_{u_k}$ and $\mathbf{c}_{\varphi_\alpha}$ are the Ritz unknown amplitudes, the vectors ϕ and ψ collect the polynomial expansion, while ω_{u_k} and ω_{φ_α} are the boundary functions, whose expression depends on the boundary condition to be imposed. In case of null displacement component along a portion or the whole boundary, the boundary functions are obtained through a combination of primitive geometries. If the edges are fully clamped, the boundary functions are set to be equal to the function representing the panel domain. In case of free edges, the boundary functions are taken equal to the unitary function. Differentiation of the boundary functions is carried out by applying the chain rule.
Due to the arbitrariness of the domains at hand, particular focus is given to the integration routine. The approach proposed in this work is based on the definition of a background mesh. First, the domain is divided into smaller elements; then, an iterative procedure is carried out to determine if the element is inside, partially inside or outside the domain. The element is halved if it falls outside the domain by an amount larger than a predefined threshold. The procedure is carried out until convergence is reached. Within each element, Gauss integration rule is used. The integration domain of the example of Eq. 5 is depicted in Fig. 3.

2.4 Asymptotic-numerical method

The asymptotic-numerical method is applied in conjunction with the Ritz method to determine the nonlinear solution. As opposed to classical predictor-corrector algorithms, the ANM employs an asymptotic expansion of the unknowns: the displacement $\mathbf{u}$ and the load parameter λ are expanded through a power series with respect to the arc-length parameter α [12]. These expansions are then substituted into the nonlinear equilibrium equations, obtaining a sequence

(a) (b)

Figure 3: Background mesh: a) integration domain; b) zoomed region

of linear problems in the unknowns $\mathbf{u}_i$ and λ_i. These problems share the same stiffness matrix, so just one matrix factorization is required during the solution process. The complete analytical representation of the nonlinear equilibrium path is obtained, as opposed to the point-by-point representation of predictor-corrector algorithms. Both a displacement-based and a mixed formulation can be introduced. The method is developed in the context of a continuation approach, so the validity of the asymptotic solution is not restricted to the neighbourhood of the starting point [13].
By assuming the existence of a critical point on the equilibrium path, $(\mathbf{u}_1, \lambda_1)$, the problem unknown $\mathbf{u}$ and the load parameter λ are expanded, in the neighbourhood of a pre-buckling solution $(\mathbf{u}_0, \lambda_0)$, in terms of a parameter α [13]:

$$\mathbf{u}(\alpha) = \mathbf{u}_0 + \alpha\mathbf{u}_1 + \alpha^2\mathbf{u}_2 + ... \tag{8}$$

$$\lambda(\alpha) = \lambda_0 + \alpha\lambda_1 + \alpha^2\lambda_2 + ... \tag{9}$$

where α is the linearized arc-length parameter. To guarantee consistency of Eqs. 8 - 9, the following orthogonality conditions are added for $p \geq 2$:

$$< \mathbf{u}_p, \mathbf{u}_1 >= 0 \tag{10}$$

where the operator $< \cdot, \cdot >$ represents the scalar product. By substituting Eqs. 8 - 9 in the governing equations, a set of linear problems is obtained. The introduction of the Ritz approximation in the linear problems and in the orthogonality conditions reads [12]:

$$\begin{bmatrix} \mathbf{K}_t(\mathbf{c}_1) & \mathbf{c}^* \\ \mathbf{c}^{*T} & 0 \end{bmatrix} \begin{bmatrix} \mathbf{c}_p \\ k \end{bmatrix} = \begin{bmatrix} -\sum_{r=1}^{p-1} \lambda_r \mathbf{K}_g \mathbf{c}_{p-r} - \mathbf{F}_p^{NL} \\ 0 \end{bmatrix} \tag{11}$$

where $\mathbf{c}_p$ is the vector of unknown amplitudes of $\mathbf{u}_p$, $\mathbf{K}_t(\mathbf{c}_1)$ is the tangent stiffness matrix at the bifurcation point, which is singular, $\mathbf{K}_g$ is the geometric stiffness matrix, $\mathbf{F}_p^{NL}$ is the Ritz discretization of the right-hand-side, and $\mathbf{c}^* = \mathbf{K}\mathbf{c}_1$, where $\mathbf{K}$ is the elastic stiffness matrix. The Lagrange multiplier k is introduced to avoid the singularity and obtain an invertible problem [12]. By solving Eq. 11 the unknowns $\mathbf{c}_p$ of the linear problems are found.
The perturbation algorithm detailed in the the previous sections allows one to determine the nonlinear solution in a neighborhood of the bifurcation point. A continuation procedure is

applied to obtain the remaining part of the branch. More details can be found in Ref. [14]. For this purpose, a new starting point is defined inside the radius of convergence and the asymptotic-numerical approach is reapplied.

3 RESULTS

This section outlines the results obtained using the R-function theory, along with the Ritz method and the asymptotic-numerical approach, to prove the capabilities of the proposed formulation. Two test cases are presented, in which laminates with different geometries, layups and fibers' orientations are analysed. The correctness of the results is checked against finite element simulations conducted using Abaqus S4R elements. In the following analyses, all the generalized displacement components are approximated using the same number of trial functions R $\times$ S. The analyses are carried out by considering different numbers of functions to perform convergence studies, while the integration grid and the number of integration points are specific for each test case. Aim of this section is to illustrate the potential of the developed formulation in handling complex domains, both from a geometrical perspective and for the enforcement of the boundary conditions. To do so, different plate configurations, boundary and loading conditions are investigated.
The material considered in the following analyses is a typical carbon/epoxy used in aerospace applications, whose elastic properties are summarized in Tab. 1. Two different panel configurations, C1 and C2, are analysed. All the relevant information are summarized below.

Table 1: Elastic properties of carbon/epoxy material

E_{11} [MPa]	E_{22} [MPa]	G_{12} [MPa]	G_{13} [MPa]	G_{23} [MPa]	ν [-]
147000	10300	7000	7000	7000	0.27

For the Newton-Raphson procedure, 100 load steps are considered; to simulate a geometrically perfect configuration, the geometric imperfection is taken with an amplitude as small as 0.1% of the thickness t. The starting point of the asymptotic procedure is the first buckling mode, which is normalized to have maximum amplitude equal to t.

Configuration C1 The first configuration is a VS square plate with a circular cutout. The plate has dimensions $a = b = 1000\ mm$, while the circular hole has radius $R = 100\ mm$ and is centered in $(x_0, y_0) = (0, 200)\ mm$. The material is the carbon/epoxy listed in Tab. 1 and 8 plies with thickness equal to $0.1272\ mm$ each and linearly varying stacking sequence $[\pm 69/\mp 5.705]_s$ are considered. The domain is obtained by combining the three primitive geometries defined in Eq. 4 according to Eq. 5.
To perform numerical integration, the domain is subdivided in 156 elements, whose size is smaller in proximity of the cutout; within each element a 4 $\times$ 4 Gauss integration rule is used, see Fig. 3.
The plate is subjected to a biaxial compression and is simply supported at the outer edges and clamped along the hole. The cutout is fixed to illustrate the potential of this approach in handling complex boundary functions. The rotations are left free in both directions.

Configuration C2 The second configuration is an I-shape plate with dimensions $a = 150\ mm$ and $b = 200\ mm$; the two square cutouts have dimensions $a_1 = a_2 = 50\ mm$ and $b_1 = b_2 = 100\ mm$ and are located in $(x_{c1}, y_{c1}) = (-50, 0)\ mm$ and $(x_{c2}, y_{c2}) = (+50, 0)\ mm$. The same material of the previous example is considered with 8 plies with total thickness equal to 1 mm and layup $[45, -45, 0, 90]_s$. For this configuration, six primitive geometries are defined:

$$\begin{aligned} \sigma_1 &= \frac{a^2 - x^2}{2a} & \sigma_2 &= \frac{a_1^2 - (x - x_{c1}))^2}{2a_1} & \sigma_3 &= \frac{a_2^2 - (x - x_{c2}))^2}{2a_2} \\ \sigma_4 &= \frac{b^2 - y^2}{2b} & \sigma_5 &= \frac{b_1^2 - (y - y_{c1}))^2}{2b_1} & \sigma_6 &= \frac{b_2^2 - (y - y_{c2}))^2}{2b_2} \end{aligned} \tag{12}$$

The final domain is obtained as:

$$\omega = ((\sigma_1 \wedge_0 \sigma_4) \wedge_0 (\overline{\sigma_2 \wedge_0 \sigma_5})) \wedge_0 (\overline{\sigma_3 \wedge_0 \sigma_6}) \tag{13}$$

For the numerical integration, 9 elements and a 30×30 Gauss integration rule are considered. A uniaxial loading condition in the y direction is considered, the plate is clamped at the bottom edge and simply supported elsewhere. A sketch of the two configurations can be found in Fig. 4, along with the boundary and loading conditions considered in the following analyses.

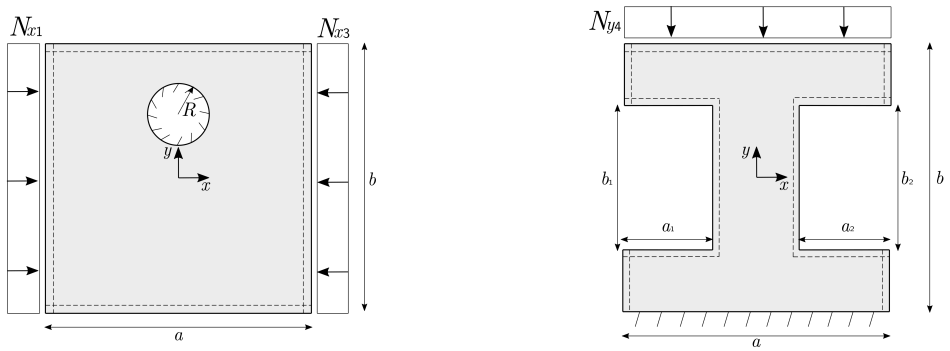

(a) (b)

Figure 4: Loading and boundary conditions: (a) Configuration C1; (b) Configuration C2

3.1 Configuration C1: postbuckling analysis

This first test case deals with the postbuckling response of Configuration C1, see Fig. 4(a). In order to determine the number of trial functions to guarantee convergence of the results, a preliminary convergence analysis is carried out. The results are summarized in Tab. 2 where the buckling multiplier, the load parameter, the maximum out-of-plane deflection and the CPU time are reported for different number of trial functions. The results obtained with the ANM are compared against Abaqus simulations. The FEM model is realized with 2667 plate elements. The mesh size has been selected after a preliminary convergence study. The fiber angle is evaluated at the center of each element and is then assumed to be constant within the element domain. The order of the perturbation expansion is set to 20, the parameter ϵ is taken equal

to 10^{-5}, 14 steps are conducted and a correction is added to the procedure. All the analyses are stopped when the load parameter λ reaches the value 1.8409, which is almost six times the critical load. The analyses are conducted with the asymptotic-numerical method, both with

Table 2: Convergence analysis for configuration C1: comparison of linearized buckling parameter, load parameter, maximum out-of-plane deflection and CPU time between ANM, NR and Abaqus (Pert. exp. = 20, $\epsilon = 10^{-5}$, Steps = 14)

			ANM_{DISP}		ANM_{MIX}		NR	
R=S	λ_{cr} [-]	λ [-]	w_{max} [mm]	t_{CPU}/t_{REF} [-]	w_{max} [mm]	t_{CPU}/t_{REF} [-]	w_{max} [mm]	t_{CPU}/t_{REF}[a] [-]
5	5.9239	1.8409	/	/	/	/	/	/
10	0.4663	1.8409	5.2413	0.5833	5.2413	0.2021	5.3257	0.6250
15	0.3128	1.8409	7.1749	0.6875	7.1749	0.5459	7.1749	0.7292
Abaqus	0.3098	1.8409	/	/	/	/	7.1750	1

[a] t_{REF} is the time employed by Abaqus simulations

a displacement and a mixed formulation, with the Newton-Raphson routine and with Abaqus simulations. As shown in Tab. 2, 5 functions in both directions lead to a buckling multiplier far from the convergence value, therefore subsequent nonlinear analyses are not carried out. On the other hand, $R = S = 15$ functions allow both the buckling multiplier and the maximum out-of-plane displacement to be captured. The results obtained with the asymptotic-numerical method closely match the reference ones obtained with Abaqus simulations, while guaranteeing improved computational times. It is interesting to point out that a mixed formulation leads to a lower CPU time.

Figure 5 illustrates the logarithm of the error between Ritz and Abaqus in terms of maximum out-of-plane displacement. The curve is plotted against the number of trial functions. As shown

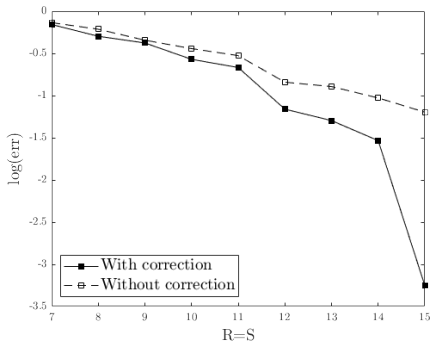

Figure 5: Maximum error of out-of-plane displacement vs number of trial functions

in Fig. 5, when a correction procedure is added to the asymptotic routine, the rate of convergence of the results is much faster than the one obtained without a correction procedure. The curve gets steeper as the number of trial functions increases.

The contour of the out-of-plane displacement at three different load levels is shown in Fig. 6. All the relevant parameters are the ones used in Tab. 2 and remain unchanged in the subsequent analyses. At each load level, the contours in Fig. 6 exhibit an excellent degree of agreement both

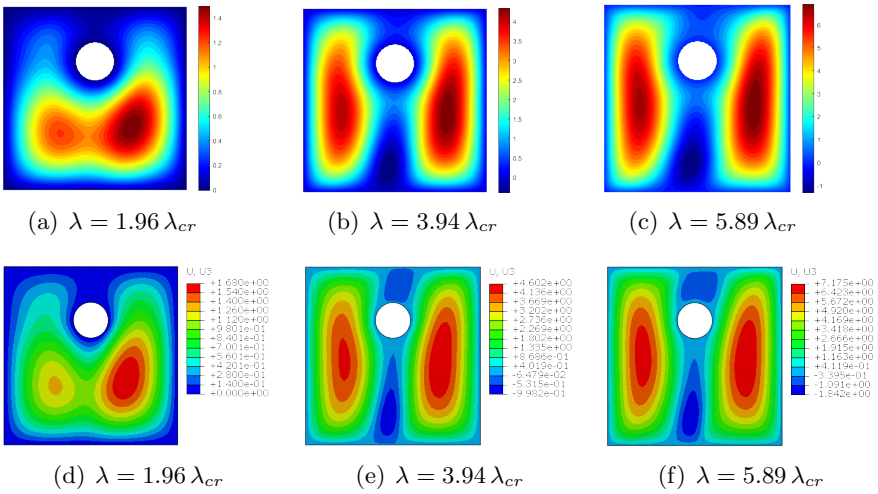

(a) $\lambda = 1.96\,\lambda_{cr}$ (b) $\lambda = 3.94\,\lambda_{cr}$ (c) $\lambda = 5.89\,\lambda_{cr}$

(d) $\lambda = 1.96\,\lambda_{cr}$ (e) $\lambda = 3.94\,\lambda_{cr}$ (f) $\lambda = 5.89\,\lambda_{cr}$

Figure 6: Out-of-plane deflections at different load levels for configuration C1: (a) - (c) ANM; (d) - (f) Abaqus

in pattern and magnitude with respect to Abaqus results. The deflected pattern experiences a progressive change of shape as the load level increases.
Lastly, the equilibrium path obtained with the ANM, NR and Abaqus is illustrated in Fig. 7 in terms of maximum out-of-plane displacement against the load parameter normalized with respect to the critical parameter. As seen, the curves are very similar, further validating the

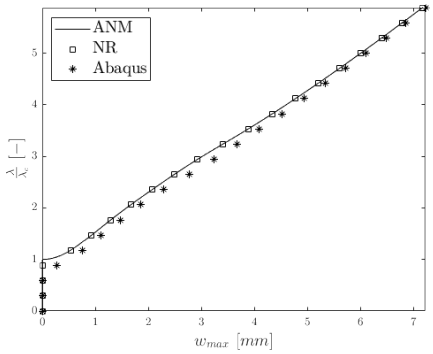

Figure 7: Force-displacement curve for configuration C1

accuracy of the predictions of the proposed formulation.

3.2 Configuration C2: postbuckling analysis

The second example regards the postbuckling response of Configuration C2; a sketch of the structure is shown in Fig. 4(b). The structure is loaded up to three times the critical load and $R = S = 25$ functions in both directions are found to be adequate for capturing the postbuckling response.
The in-plane and out-of-plane displacement components are reported in Fig. 8. Both the in-plane and out-of-plane displacement components are correctly captured, as revealed by the

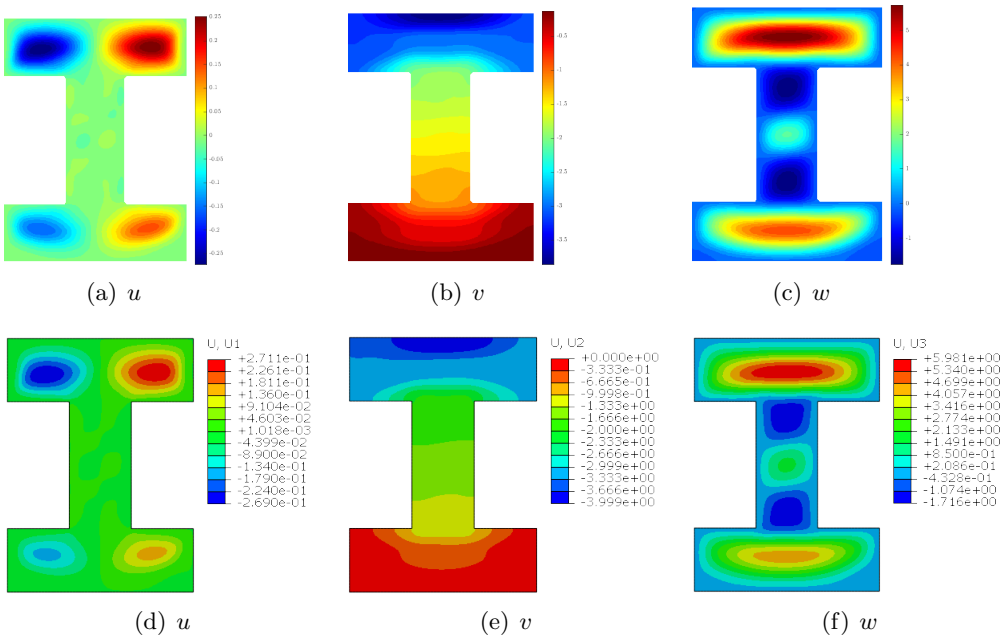

(a) u (b) v (c) w

(d) u (e) v (f) w

Figure 8: In-plane and out-of-plane displacements for configuration C2: (a) - (c) ANM; (e) - (f) Abaqus

comparison with Abaqus simulations. The postbuckling shape exhibits a complex pattern with five waves in the load direction.

The membrane forces resultants contour is shown in Fig. 9, where Ritz approach is compared with FEM results. The contours reveal an axial resultant N_{xx} which is tensile in the central regions, with negative peaks at the corners; while the transverse resultant N_{yy} exhibits a redistribution towards the edges. The shear resultant is characterized by a relatively complex shape, proving the ability of the method to precisely capture the postbuckling response of the structure.

4 CONCLUSIONS

A formulation based on the combined use of the Ritz method, the asymptotic-numerical method and R-functions is presented for the postbuckling analysis of variable stiffness plates with arbitrary geometries. The proposed approach is promising for its high computational efficiency combined to its reduced modelling efforts. This is particularly suitable for the analysis of arbitrarily shaped domains. The use of R-functions allows a wide variety of domains to be handled, while a Ritz-based model allows for a much smaller number of degrees of freedom with respect to finite element models with comparable accuracy. A not negligible computational time is required when refined Ritz expansions are needed unless proper care is taken. In this regard, the ANM is a powerful strategy to overcome this issue. In particular, this method offers a number of interesting features: a lower computational time, a larger range of validity of the solution with respect to a simple linearization and a complete analytic representation of the nonlinear equilibrium path. The tool can be exploited in future works to conduct parametric studies on the fibers' path to achieve better load redistribution and to perform preliminary studies to optimize the stiffness tailoring in the postbuckling field. The proposed strategy can be further

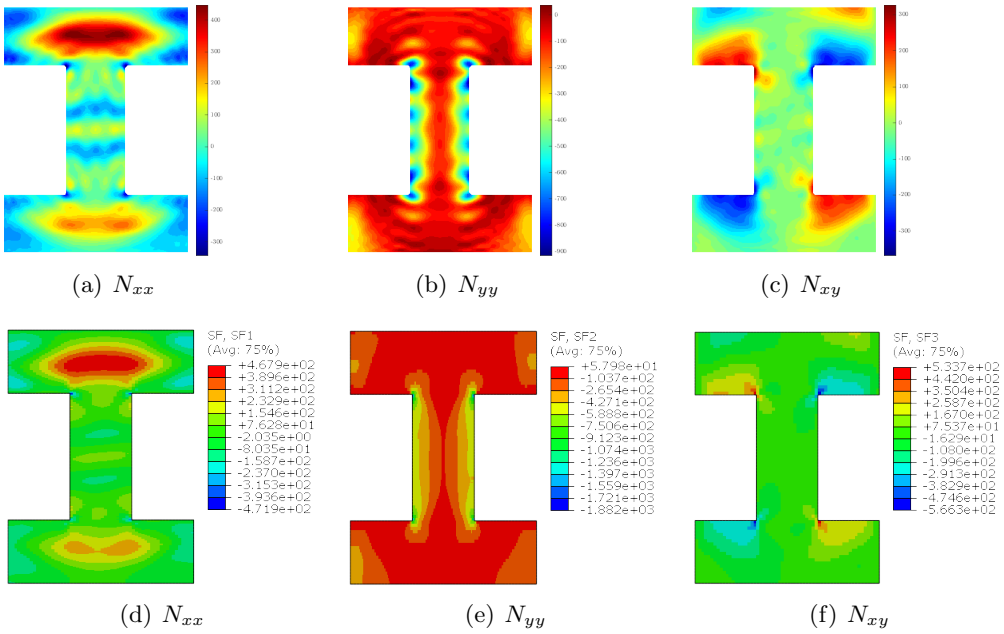

(a) N_{xx} (b) N_{yy} (c) N_{xy}

(d) N_{xx} (e) N_{yy} (f) N_{xy}

Figure 9: Membrane resultants for configuration C2: (a) - (c) ANM; (e) - (f) Abaqus

extended by considering shell-like panels and other thermo-mechanical loading conditions. The addition of curvilinear stiffeners to the panel is another interesting subject to be addressed in future works.

References

[1] Z. Gürdal and R. Olmedo 1993. "In-Plane Response of Laminates with Spatially Varying Fiber Orientations–Variable Stiffness Concept". AIAA Journal, 31, no. 4: 751–758. https://doi.org/10.2514/3.11613

[2] B. Coburn and P. Weaver 2016. "Buckling Analysis, Design and Optimisation of Variable Stiffness Sandwich Panels". International Journal of Solids and Structures, 96: 217-228. https://doi.org/10.1016/j.ijsolstr.2016.06.007

[3] R. Vescovini and L. Dozio 2016. "A Variable-Kinematic Model for Variable Stiffness Plates: Vibration and Buckling Analysis". Composite Structures, 142: 15–26. https://doi.org/10.1016/j.compstruct.2016.01.068

[4] V. Oliveri, A. Milazzo and P. Weaver 2018. "Thermo-Mechanical Post-Buckling Analysis of Variable Angle Tow Composite Plate Assemblies". Composite Structures, 183: 620–635. https://doi.org/10.1016/j.compstruct.2017.07.050

[5] G. Sciascia, V. Oliveri, A. Milazzo and P. Weaver 2020. "Ritz Solution for Transient Analysis of Variable-Stiffness Shell Structures". AIAA Journal, 58, no. 4: 1796–1810. https://doi.org/10.2514/1.J058686

[6] R. Vescovini, E. Spigarolo, E. Jansen and L. Dozio 2019. "Efficient Post-Buckling Analysis

of Variable-Stiffness Plates Using a Perturbation Approach". Thin-Walled Structures, 143: 106211. https://doi.org/10.1016/j.tws.2019.106211

[7] W. Zhao and R. K. Kapania 2019. "Prestressed Vibration of Stiffened Variable-Angle Tow Laminated Plates". AIAA Journal, 57, no. 6: 2575-2593. https://doi.org/10.2514/1.J057719

[8] A. Pagani and A. Sanchez-Majano 2020. "Influence of Fiber Misalignments on Buckling Performance of Variable Stiffness Composites Using Layerwise Models and Random Fields". Mechanics of Advanced Materials and Structures, 57, no. 6: 1–16. https://doi.org/10.1080/15376494.2020.1771485

[9] V. Rvachev, T. Sheiko and V. Shapiro 1999. "The R-Function Method in Boundary-Value Problems with Geometric and Physical Symmetry". Journal of Mathematical Sciences, 97, no. 1: 3888–3899. https://doi.org/10.1007/BF02364929

[10] R. Vescovini 2023. "Ritz R-function Method for the Analysis of Variable Stiffness Plates". AIAA Journal, 61, no. 6: 2689–2701. https://doi.org/10.2514/1.J062702

[11] N. Damil and M. Potier-Ferry 1990. "A New Method to Compute Perturbed Bifurcations: Application to the Buckling of Imperfect Elastic Structures". International Journal of Engineering Science, 28: 943-957. https://doi.org/10.1016/0020-7225(90)90043-I

[12] B. Cochelin, N. Damil and M. Potier-Ferry 1994. "Asymptotic-Numerical Methods and Padé Approximants for Non-linear Elastic Structures". International Journal for Numerical Methods in Engineering, 37: 1187- 1213. https://doi.org/10.1002/nme.1620370706

[13] B. Cochelin, N. Damil and M. Potier-Ferry 1994. "The Asymptotic-Numerical Method: An Efficient Perturbation Technique for Nonlinear Structural Mechanics". Revue Européenne des Éléments Finis, 3, no. 2: 281-297. https://doi.org/10.1080/12506559.1994.10511124

[14] B. Cochelin 1994. "A Path-Following Technique via an Asymptotic-Numerical Method". Computers & Structures, 53, no. 5: 1181-1192. https://doi.org/10.1016/0045-7949(94)90165-1

[15] L. Azrar, B. Cochelin, N. Damil and M. Potier-Ferry 1993. "An Asymptotic-Numerical Method to Compute the Postbuckling Behavior of Elastic Plates and Shells". International Journal for Numerical Methods in Engineering, 36: 1251-1277. https://doi.org/10.1002/nme.1620360802

[16] M. Potier-Ferry and J. M. Cadou 2004. "Basic ANM Algorithms for Path Following". Revue Européenne des Éléments Finis, 13: 9-32. https://doi.org/10.3166/reef.13.9-32

[17] R. Vescovini, V. Oliveri, D. Pizzi, L. Dozio and P. M. Weaver 2020. "A Semi-Analytical Approach for the Analysis of Variable-Stiffness Panels with Curvilinear Stiffeners". International Journal of Solids and Structures, 188-189: 244-260. https://doi.org/10.1016/j.ijsolstr.2019.10.011

[18] R. Vescovini and P. P. Foligno 2023. "Fast Analysis of Curvilinearly Stiffened Panels Operating in the Postbuckling Field". Mechanics of Advanced Materials and Structures, 30, no. 5: 1009-1030. https://doi.org/10.1080/15376494.2022.2135146